Spectral Imaging for Microbubble Characterisation

*Richard J Browning[1], Miles Aron[1], Anna Booth[1,2], Paul Rademeyer[1], Sarah Wing[1], Veerle Brans[1], Shamit Shrivastava[1], Dario Carugo[1,3], Eleanor Stride[1]**

[1] Department of Engineering Science, Institute of Biomedical Engineering, University of Oxford, Oxford OX3 7DQ, United Kingdom.

[2] Department of Chemistry, University of Oxford, Oxford OX1 3QR, United Kingdom.

[3] Faculty of Engineering and Physical Sciences, University of Southampton, Highfield, Southampton SO17 1BJ, United Kingdom.

* eleanor.stride@eng.ox.ac.uk

Keywords: microbubbles, spectral imaging, Laurdan, ultrasound, drug delivery, contrast agents

ABSTRACT

Microbubbles stabilised by an outer lipid shell have been studied extensively for both diagnostic and therapeutic applications. The shell composition can significantly influence microbubble behaviour, but performing quantitative measurements of shell properties is challenging. The aim of this study was to investigate the use of spectral imaging to characterise the surface properties of a range of microbubble formulations representing both commercial and research agents. A lipophilic dye, C-Laurdan, whose fluorescence emission varies according to the properties of the local environment, was used to compare the degree and uniformity of lipid order in the microbubble shell and these measurements were compared with the acoustic response and stability of the different formulations.

The method was found to be suitable for performing rapid and hence relatively high throughput measurements of microbubble surface properties. Interestingly, despite significant differences in lipid molecule size and charge, all of the different formulations exhibited highly ordered lipid shells. Measurements of liposomes with the same composition and the debris generated by destroying lipid microbubbles with ultrasound showed that these exhibited a lower and more varied lipid order than intact microbubbles. This suggests that the high lipid order of microbubbles is due primarily to compression of the shell as a result of surface tension and is only minimally affected by composition. This also explains the similarity in acoustic response between the formulations since microbubble dynamics are determined by the diameter and shell viscoelastic properties that are themselves a function of lipid order. Within each population, there was considerable variability in lipid order and response between individual microbubbles, suggesting the need for improved manufacturing techniques. In addition, the difference in lipid order between the shell and lipid debris may be important for therapeutic applications in which shedding of shell material is exploited e.g. for drug delivery.

INTRODUCTION

Contrast agents for ultrasound imaging consist of suspensions of gas microbubbles stabilised by a shell of lipid, protein or polymer surfactants, and ranging in diameter from ~1-10 μm [1]. Their clinical utility lies in their combination of echogenicity and highly nonlinear behaviour upon ultrasound (US) exposure, which facilitates measurement of tissue perfusion [2], blood flow velocity [3], and identification of potential sites of haemorrhage [4] or stenosis [5]. Additionally, much research has gone into potential therapeutic applications of microbubbles, due to their ability to produce highly localised biophysical effects, including enhanced drug uptake and both mechanical and thermal ablation [6-7].

As the sphere of microbubble usage expands, there is an increasing need to understand how their physical properties affect behaviour and function. The shell has a strong influence on microbubble behaviour [8-10]; but quantitative measurement of shell parameters, such as elasticity, viscosity, density and structure, i.e. lamellarity, presents a considerable challenge. Several studies have also shown that there can be considerable variability in the behaviour of individual microbubbles across a population, independent of their size [11-14]. Consequently, methods are required that can characterise the shell properties of large quantities of single microbubbles.

Various fluorescence microscopy techniques have been applied to microbubble characterisation. Conjugation of fluorescent compounds to shell components or use of lipophilic dyes (i.e. lipid analogue dyes) have allowed qualitative visualisation of phase separation effects of different coating components and production methods [13]. These techniques allow direct visualisation of targets of interest, but the addition of large fluorescent groups can alter the behaviour of the conjugated molecule. Additionally, photobleaching and preferential partitioning of dyes [15-16] may affect image interpretation.

Quantitative or semi-quantitative fluorescence techniques have also been used to probe microbubble shell properties. Hosny et al. used boron-dipyrromethene (BODIPY)-C_{10} molecular rotors to investigate differences between microbubbles fabricated by sonication or by microfluidics [11]. BODIPY-C_{10} is a lipophilic dye whose quantum yield decays during Fluorescence Lifetime Imaging Microscopy (FLIM) varies depending upon local viscosity, allowing investigation of the variation of viscosity over the surface of an individual microbubble or across a population. FLIM allows quantitative assessment of viscosity, but temporal resolution and throughput is low, as multiple photon excitations are required to reduce noise, and only large bubbles (>20μm in diameter) outside the desired clinical size range have so far been characterised successfully.

Fluorescence Recovery After Photobleaching (FRAP) has also been used to measure the diffusion kinetics of dye-conjugated lipids within the shells of microbubbles of clinically relevant sizes [12]. By photobleaching an area and measuring the time it takes for the fluorescent signal to be restored, the viscosity of the shell can be calculated. However, this technique requires bubbles to remain stationary during investigation, and again as for FLIM, temporal resolution and throughput are low. Additionally, as only discrete regions of the bubble are bleached, variations across the bubble shell cannot be not fully resolved.

In this work we investigate the potential use of C-Laurdan, a lipophilic, polarity sensitive dye for the characterisation of lipid coated microbubbles. C-Laurdan is a carboxylate modified derivative of Laurdan, but offering improved solubility, photostability and polarity sensitivity [17]. Both dyes preferentially stain lipid environments, and their emission spectrum is a function of the thermodynamic state of the lipid interface. In particular, a decrease in the order (i.e. an increase in degrees of freedom) of the lipid molecules results in a red-shift in the emission spectra of C-Laurdan. A measure of lipid order, known as Generalized Polarization (GP) [18], can be determined from the fluorescence intensities at the maximum emission wavelengths in

the gel phase and liquid-crystalline phase (see Equation 1). Since lipid order is a function of the thermodynamic state of the system, the observed GP can be related to the physical properties of the microbubble shell. The observed GP thus allows a comparison of shell properties across different lipid formulations, temperatures, suspending medium conditions, etc.:

Equation 1

$$GP = \frac{(I_{440} - I_{490})}{(I_{440} + I_{490})}$$

where I_{440} is the fluorescence intensity at 440 nm, and I_{490} is the fluorescence intensity at 490 nm.

Equation 1 was derived for Laurdan but the dielectric relaxation mechanism by which both Laurdan and C-Laurdan respond to their environment is fundamentally the same. The differences in their structures however, requires that they are calibrated separately. For the purposes of this study, an empirical relationship between GP and lipid order is required. This relationship has been obtained and compared for Laurdan and C-Laurdan previously by others [19]. It has also been shown previously that the emission spectrum and GP of Laurdan is related to the compressibility of lipid shells in multi-lamellar vesicles, independent of the lipid composition [20].

The use of spectral analysis and GP to investigate microbubble shell lipid order has several potential advantages. First, a relatively high throughput is achievable as the technique relies solely on fluorescence intensity measurements and multiple microbubbles can therefore be imaged in a single frame. Second, the measurements can be taken rapidly as only two wavelengths are required. This again increases throughput, avoids the need for fixation of the microbubble to a surface which may affect shell properties, and allows imaging of smaller microbubbles which are more strongly affected by Brownian motion. Third, as GP is a spectral

ratio, intensity variation between formulations does not impact the results as significantly as in other methods. Fourth, C-Laurdan has minimal preferential interaction with specific lipids, producing homogenous staining of membranes and potentially allowing visualisation of local domains across an individual microbubble shell [11, 13]. C-Laurdan spectral imaging can also be combined with fluorescence correlation spectroscopy for improved temporal and spatial resolution [21], although this approach does require the microbubbles to be stationary for longer periods.

Microbubbles have been previously imaged using Laurdan by Slenders et al., who stained DPPC coated microbubbles containing perfluorobutane gas. They found that large microbubbles (dia. >50 μm) initially had a low GP value, indicating a disordered membrane with low lipid order. Over time, the microbubbles gradually decreased in size, due to diffusion of gas into the surrounding liquid. This increased the surface density of lipid molecules and re-organisation of the shell into a gel phase as evidenced by a spectral blue-shift in the Laurdan emission and hence higher GP values. Eventually, the microbubbles reached a stable state in terms of both size and lipid order. Considering that clinically relevant microbubbles are <10 μm, these results suggest that the shells of such microbubbles should be in a highly ordered state; however the effect of other microbubble components, such as emulsifiers, was not investigated.

In the present study, to investigate the utility of spectral imaging for microbubble characterisation, five lipid-based microbubble formulations, representing both research and commercial agents, were prepared and stained with C-Laurdan dye for confocal microscope imaging. Equivalent formulations of liposomes and the debris generated by destroying microbubbles with ultrasound were also characterised in the same way. The size, concentration, stability and acoustic response of the microbubble formulations were then measured to determine whether there was a correlation between GP and microbubble properties.

MATERIALS AND METHODS

Materials

The lipids 1,2-dipalmitoyl-sn-glycero-3-phosphocholine (DPPC, 850355), 1,2-distearoyl-sn-glycero-3-ethylphosphocholine (DSEPC, 890703), 1,2-dipalmitoyl-sn-glycero-3-phosphate (DPPA, 830855), 1,2-distearoyl-sn-glycero-3-phosphoethanolamine-N-[methoxy (polyethylene glycol)-5000] (DSPE-PEG5K, 880220) and 1,2-distearoyl-sn-glycero-3-phosphocholine (DSPC, 850365) were purchased from Avanti Polar Lipids, Inc. (Alabaster, AL, USA) as a 25 mg/mL solution in chloroform, except for DPPA which was a powder. Polyoxyethylene (40) stearate (PEG-40S) was purchased from Sigma-Aldrich Company Ltd (Dorset, UK) as a powder. SonoVue® was purchased from Bracco UK Limited, High Wycombe, UK. Dulbecco Phosphate-Buffered Saline (PBS) was purchased from ThermoFisher Scientific (Waltham, MA, USA). The membrane polarity dye, 6-dodecanoyl-2-[N-methyl-N-(carboxymethyl) amino]naphthalene (C-laurdan) was purchased from TP Probes (Ochang-eup, Korea) and received as a kind gift from Dr Erdinc Sezgin (Weatherall Institute of Molecular Medicine, University of Oxford, Oxford, UK). Unless otherwise stated, all other chemicals were purchased from Sigma-Aldrich Company Ltd.

Production of lipid microbubbles

All microbubbles, except SonoVue®, were initially prepared as thin dried films from lipids dissolved in chloroform, typically either purchased or prepared to 25 mg/mL, except for PEG-40S (10 mg/mL in chloroform) and DPPA (5 mg/mL in methanol:chloroform:water, at 65:35:4 v/v). For each formulation, lipids were mixed at the molar ratios shown in Table 1, and left to evaporate to a thin film in a glass vial covered with perforated Parafilm (Bemis Company, Inc., Neenah, WI, USA). The total weight of lipids per film was 20 mg.

Lipid films were then resuspended in 5 mL Dulbecco's phosphate-buffered saline (PBS, Life Technologies, Paisley, UK) and stirred at 100°C on a magnetic stirrer hotplate for a minimum of 30 minutes. The lipids were then homogenously dispersed within the solution by sonication for approximately 2.5 minutes using a micro-sonicator tip fully immersed in the solution at a power setting of 3 (Microson XL 2000, QSonica, Newtown, CT, USA). The sonicator tip was then moved to the air-liquid interface and the headspace in the vial filled with sulphur hexafluoride (SF_6) (The BOC Group, Guildford, UK). The solution was again sonicated under constant sulphur hexafluoride flow for 30 seconds at a power setting of 14 to form a cloudy suspension of microbubbles. The vial was immediately placed in ice to cool and then capped.

SonoVue®, a lipid shelled microbubble of SF_6 gas provided as a cake of lyophilised powder, was reconstituted according to the manufacturer's instructions using the supplied 5 mL of saline. It should be noted that the commercial agent Definity® (Lantheus Medical Imaging), is prepared by mechanical agitation in an atmosphere of perfluorobutane. Microbubbles with the same lipid composition (D-L) were utilised for this study but prepared by sonication as above using SF_6, and the lipid film was resuspended in a solution of water:glycerol:propylene glycol (80:10:10, v/v). Table S2 in the supporting information provides a summary of the differences between the lipid molecules. Table S3 provides the molar concentrations of each lipid.

Preparation of liposomal vesicle suspensions

Liposomal vesicle suspensions of the DPPC formulation were prepared to enable comparison between their surface properties and those of microbubbles. Additionally, a series of liposomes consisting of a single phosphatidylcholine lipid species of varying chain length, without the addition of PEG40S, were prepared for the high-speed GP measurements in the flow chamber set up described below. Liposomes were prepared by the same method as microbubbles but

without the final sonication in the presence of gas. Without further processing, liposomes prepared in this manner are expected to have a mixture of sizes and lamellarity.

Table 1: Constituents of the microbubble formulations used. *Abbreviations: DPPG: 1,2-dipalmitoyl-sn-glycero-3-phospho-(1'-rac-glycerol), PA: palmitic acid, DPPC: 1,2-dipalm itoyl-sn-glycero-3-phosphocholine, DSEPC: 1,2-distearoyl-sn-glycero-3-ethyl phospho choline, DPPA: 1,2-dipalmitoyl-sn-glycero-3-phosphate, DSPE-PEG5K: 1,2-distearoyl-sn-glycero-3-phosphoethanolamine-N-[methoxy(polyethylene glycol)-5000], DSPC: 1,2-distearoyl-sn-glycero-3-phosphocholine, PBS: phosphate-buffered saline, PEG40S: polyoxyethylene (40) stearate.*

Formulation	Constituents	Molar Ratio	Suspending medium
DPPC	DPPC : PEG40S	9 : 1	PBS
DSEPC	DSPC : DSEPC : PEG40S	19.3 : 9 : 1	PBS
DSPC	DSPC : PEG40S	9 : 1	PBS
SonoVue®	DSPC : DPPG : PA : Macrogol 4000	71 : 75 : 46 : 9806	0.9% Saline
D-L	DPPC : DPPA : DSPE-PEG5K	8 : 1 : 1	Water : Glycerol : Propylene Glycol

Microbubble concentration, size and stability analysis

Population statistics – defined here as microbubble concentration, mean diameter and median diameter – were collected using an electrozone sensing approach (Coulter Multisizer 4e, Beckman Coulter, Opa Locka, FI) as described in Feshitan et al. [22]. Briefly, freshly prepared microbubbles were homogenously dispersed by gentle agitation. 2 µL of microbubbles were

diluted into 10 mL of Isoton II in an accuvette. A 20-µm aperture (size range of 0.4 – 16 µm) was used for the measurements. Samples were measured at t = 0, 30, 60 and 90 minutes and all samples were measured at least three times per time point. Approximately 2000-45000 microbubbles were imaged per sample dependent on initial concentration (6000-135000 per formulation).

For stability analysis, population statistics were obtained as described above over 90 minutes. From these results, changes in concentration and size were examined. This was repeated two to three times using a fresh bubble suspension created from a new lipid film each time. Bubble suspensions were uncapped and allowed to warm up to room temperature (~18-22 ^{o}C) before commencing measurements.

C-Laurdan staining and microbubble washing

Microbubble lipid order was examined by C-Laurdan staining and GP analysis. To reduce background fluorescence from unincorporated lipids in the suspension, microbubbles were washed once by centrifugation. Approximately 3 mL of freshly prepared microbubbles were loaded into a disposable 10 mL syringe adapted to fit upright within a 50 mL centrifuge tube and spun at 1000g relative centrifugal force (RCF) at 10 ^{o}C for 10 minutes in a swing bucket rotor (Heraeus Labofuge 400R, Thermo Scientific) to form a microbubble cake against the plunger. The subnatant was discarded and the microbubbles resuspended within the syringe using 2 mL of the original suspending medium (Table 1). This was then transferred to a glass vial for future use. For C-Laurdan staining, 1.5 to 5 µL of 1 mM C-Laurdan was added to 30 µL of washed microbubbles diluted in 70 µL Milli-Q water (total volume 100 µL) and incubated for 30 minutes at 4^{o}C before use. It should be noted that this would be a minimum of 15 µM of C-Laurdan per sample. However, no significant differences between GP values were found from 1 to 15 µM (data not shown). In addition, intensity values for microbubbles

stained with concentrations of 0.2 μM C-Laurdan were close to the detection threshold particularly in the 490 nm range.

For the measurements of liposome and microbubble GP using the flow chamber setup, 0.6 μL C-Laurdan was added to either 100 μL of the liposome stock solution diluted in 1.4 mL Milli-Q water, or 500 μL of the microbubble stock solution diluted in 1.0 mL Milli-Q water (both with total volume 1.5 mL). Removal of lipid refuse from the microbubble samples in this setup was achieved by allowing the microbubbles to float into and adhere to the upper film enclosing the flow chamber, and then flowing an additional 1.0 mL Milli-Q water at 20 mL/hr to clear away unbound lipids and C-Laurdan. Optical inspection revealed that this technique lowered background fluorescence to control levels while retaining C-Laurdan-labelled microbubbles at the upper film of the flow chamber.

Spectral fluorescence imaging on static (i.e. no flow) samples

Spectral imaging was performed on an inverted confocal microscope (LSM 780, Carl Zeiss Microscopy GmbH, Jena, Germany) using a previously reported method [23]. Briefly, 10 μL of stained microbubbles was loaded onto a 170 μm-thick glass slide and covered with a cover slip. Individual microbubbles were then located and imaged using an oil immersion 63x objective. Microbubbles float up to the cover slip surface and the microscope focus was set at the midplane of the microbubbles, however as the confocal microscope has a short z-axis focal length and the microbubbles have a disperse size distribution, only a subset of microbubbles sizes can be imaged at their midplane. To overcome this, each image was captured at different locations and different z-positions to capture a range of microbubble sizes at their midplanes for analysis. Out-of-plane microbubbles were excluded during the semi-automated image processing mentioned below. C-Laurdan dye was excited using the 405 nm laser and spectral images from 421 to 680 nm, in ~9 nm steps, were captured on a Gallium Arsenide Phosphide

(GaAsP) spectral detector using the native microscopy software (Zen Black, Carl Zeiss Microscopy GmbH, Jena, Germany). This resulted in a single stacked image, with each stack corresponding to the intensity image at a single wavelength (n=30). Approximately 20 images were taken per formulation and each formulation was repeated three times using a freshly prepared microbubble suspension created from a new lipid film. Depending upon the concentration and formulation, an average of ~490 microbubbles were imaged per sample and an average of ~1460 microbubbles were imaged per formulation. All imaging was performed at room temperature. Fluorescence images were then processed using a custom script (See SI).

Measurements in the flow chamber setup

Microbubble samples were loaded into a flow chamber at the focus of a co-aligned acoustic and optical setup designed to measure GP during ultrasound exposure (See SI for details). First, GP measurements were performed on the loaded chamber without ultrasound and an image was captured by camera to ensure that the microbubbles were in focus. Samples were then exposed to ultrasound bursts (500 kHz, 100 mV peak to peak, 0.6 MPa peak negative pressure, continuous wave) while the fluorescence emissions from C-Laurdan were recorded using two photomultiplier tubes (PMT)s and the acoustic emissions were monitored using a single element ultrasound transducer (V320 Panametrics, Olympus, centre frequency 7.5 MHz) as a passive cavitation detector (PCD). Following ultrasound exposure, GP measurements were again performed, and alignment verified by camera to ensure that the optics were aligned with the area where the microbubbles were destroyed. If the ultrasound and optical focuses were not aligned, the alignment was adjusted and a post-exposure measurement was still taken; however, only pre- and post-ultrasound data were analysed. If still aligned, the real-time data taken during ultrasound exposure was also analysed. The same method was used to measure GP of

the liposome samples. In this case the liposomes (<500 nm in diameter) were not directly imaged. It should also be noted that changes in the optical setup or intermediate surfaces between the sample and the measurements produces a fixed offset in GP values. Therefore, absolute GP values cannot be compared between different optical setups without extensive calibration. Changes in GP values are, however, comparable and it is these that are measured in this study.

Single microbubble acoustic response

The response of individual microbubbles to ultrasound excitation was measured using the apparatus described Rademeyer et al. [14]. Briefly, a dilute suspension of microbubbles was focussed into a stream of single microbubbles by hydrodynamic flow focussing using a microfluidic device. This stream was directed through the coaligned foci of an ultrasound transducer and a microscope objective in a large water tank so that the microbubble was at least 100 µm from any boundary. Details of the alignment process and associated uncertainty may be found in Rademeyer et al. The microbubble was illuminated using a laser (405 nm, 4.5mW, Thorlabs) and the 90^{o} scattered light from the microbubbles was detected by a photomultipler tube (H10493-003, Hamamatsu Photonics) through a water submersible 40x objective (LUMPLFLN 40XW, Olympus) and signal traces recorded on an oscilloscope (Waverunner 64Xi, Lecroy). As individual microbubbles crossed the laser focus, a function generator (33220A, Agilent) sent a driving waveform through a 50 dB amplifier (325LA, E&I) to a 3.5 MHz focused ultrasound transducer (Panametrics NDT, Waltham, MA, USA). The resultant microbubble oscillations were detected by the PMT as fluctuations in laser scatter. Microbubbles of the different formulations were probed using single 5 cycle ultrasound pulses of 3.5 MHz centre frequency and with peak negative pressures from 0 to 300 kPa (separate experiments were conducted for each pressure).

RESULTS

Microbubble production and stability

The population characteristics for each of the formulations are shown in Figure 1. Immediately following production, all in-house formulations were found to have a high concentration (>1x10^9 microbubbles/ml) with a mean diameter between 1 and 2 µm. SonoVue microbubble concentrations were within the reported 2-5 x 10^8 microbubbles/mL range [24], whereas DPPC microbubbles had an mean concentration of 5 x10^8 microbubbles/mL and an mean initial diameter of ~3 µm. Interesting to observe is the multimodal size distribution as obtained for DPPC, with the first second peak located at ~5 µm.

The changes in size and concentration over 90 mins for each of the formulations are shown in Figure 2. DSPC, DSEPC and SonoVue microbubbles exhibited minimal changes in size (<5%) over this time and SonoVue microbubbles were also stable in terms of concentration (maximum change of 3%). DPPC microbubbles underwent an initial decrease in concentration (~18%) after which they stabilised, and a gradual decrease in size of ~6%. DSEPC microbubbles exhibited a gradual ~9% drop in concentration over the course of 90 min, whereas DSPC bubbles exhibited an initial ~12% drop in concentration, after which they the concentration remained stable. D-L microbubbles showed a gradual decrease in mean diameter (~9%) and a gradual increase in concentration (~20%) over 90 minutes, which may have indicated dissolution of microbubbles and/or microbubble fusion. None of the formulations showed a significant difference in concentration or size compared at any timepoint on a repeated measures two-way ANOVA, with multiple comparison between time and formulation (PRISM 6, GraphPad Software), with the exception of DSPC vs. D-L at t = 90 min ($p < 0.05$).

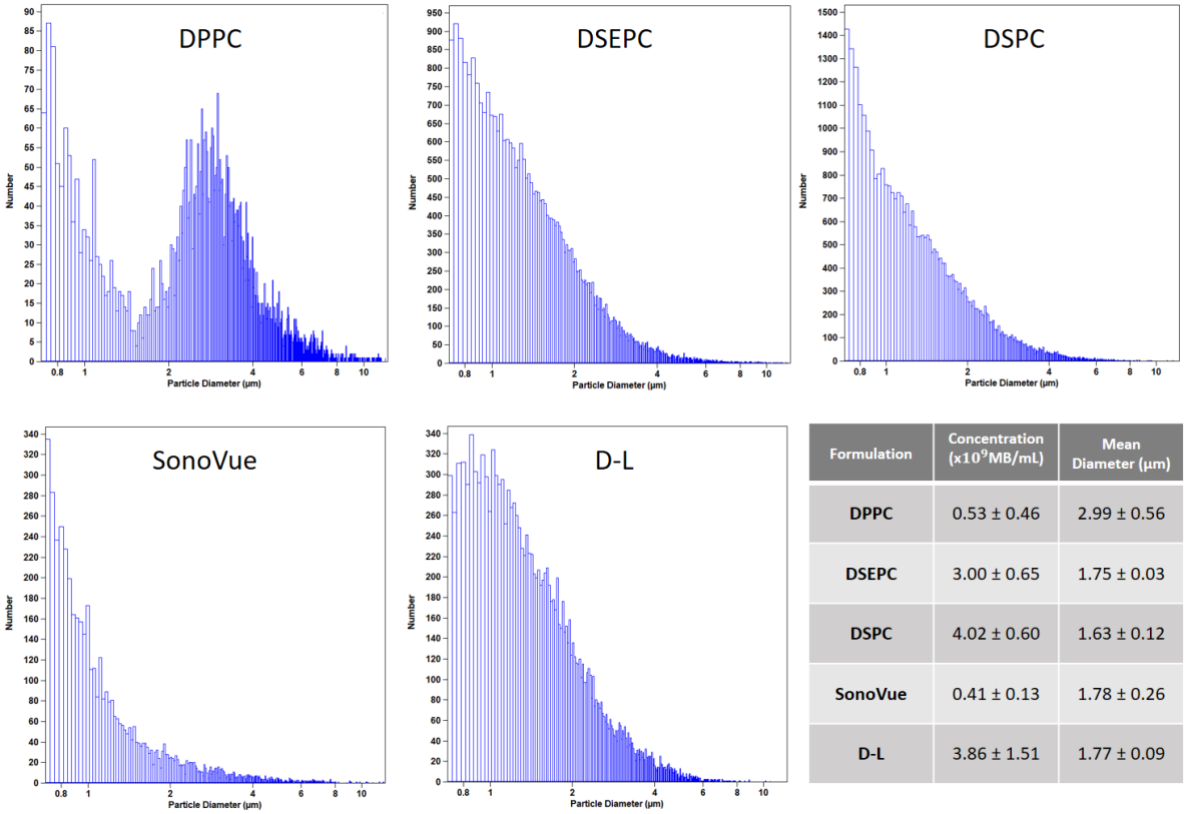

Formulation	Concentration ($\times 10^9$MB/mL)	Mean Diameter (µm)
DPPC	0.53 ± 0.46	2.99 ± 0.56
DSEPC	3.00 ± 0.65	1.75 ± 0.03
DSPC	4.02 ± 0.60	1.63 ± 0.12
SonoVue	0.41 ± 0.13	1.78 ± 0.26
D-L	3.86 ± 1.51	1.77 ± 0.09

Figure 1: Population statistics of the microbubble formulations. Histograms at t = 0 min of the 5 formulations are shown, with particle diameter on the x-axis and raw number of particles on the y-axis. The inset table shows the concentration and mean diameter (± standard deviation) from 2 to 3 independent samples for each formulation. A minimum of 2000, up to a maximum of 40,000 microbubbles were measured to determine population statistics for the formulations.

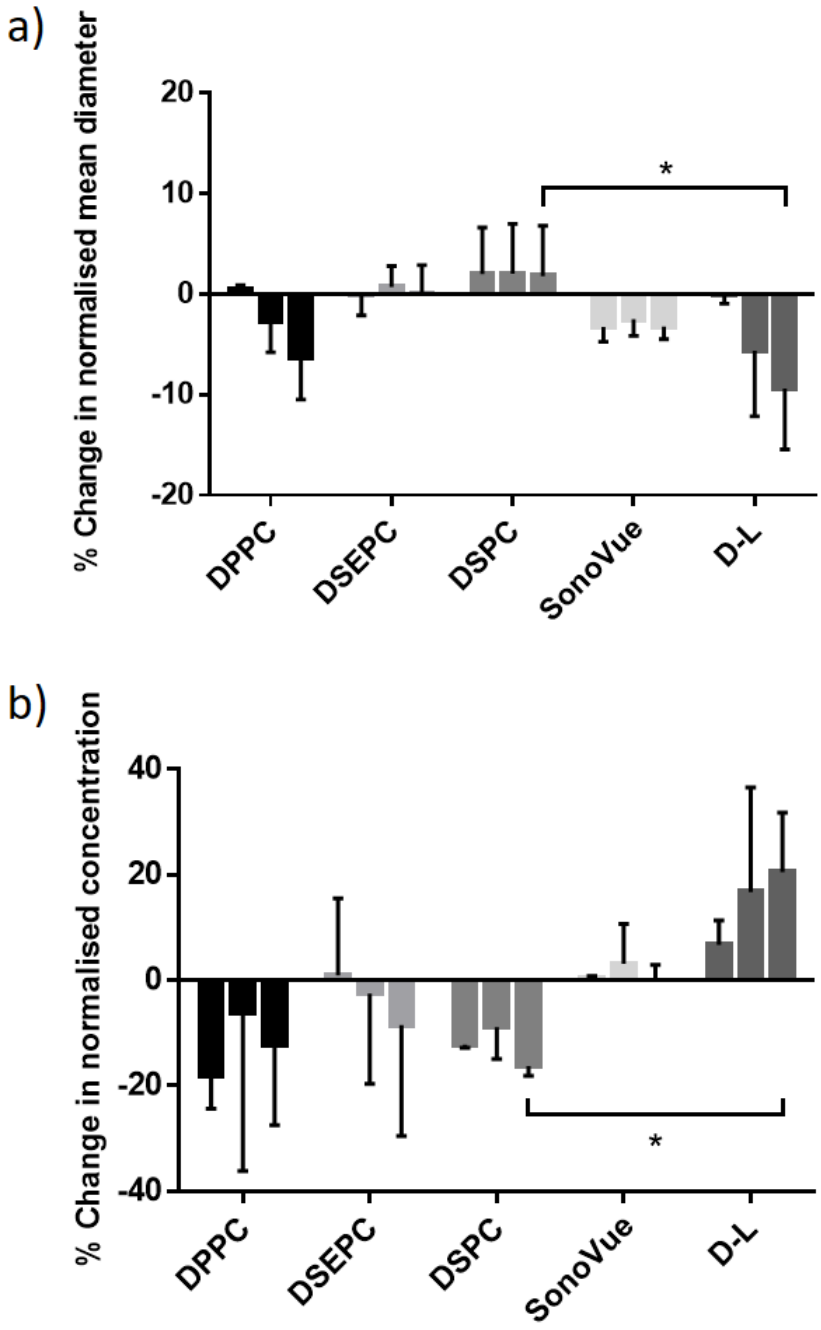

Figure 2: Percentage change in population statistics of microbubbles measured over 90 min. Microbubble samples were extracted from an open vial stored at the ambient temperature and pressure at fixed time points (0, 30, 60 and 90 minutes) and their size distribution and concentration measured using the Multisizer. (a) Concentration and (b) mean diameter (µm) are normalised to their values at time 0 and expressed as a percentage. For each microbubble type, the bars left to right represent 30, 60 and 90 minutes.

Lipid order of microbubbles under static conditions

C-Laurdan GP values of microbubbles extracted from spectral image stacks acquired by fluorescence microscopy were averaged and weighted to give an average GP per formulation (Table 2). Example images of microbubbles and associated histograms of GP values per pixel are shown in Figure S1. GP values were ordered from highest to lowest as D-L > DSEPC > SonoVue > DSPC > DPPC. Mean values are shown in Figure 3. Groups were compared by one way ANOVA and found to be significantly different ($p<0.01$). Multiple comparisons by a Tukey test revealed a statistically significant difference for D-L vs DPPC ($p<0.01$) and D-L vs DSPC ($p<0.05$) formulations. The confidence intervals are given in Figure S6.

The dependence of the measured GP values on microbubble size was investigated by measuring the diameter of each microbubble in the spectral images (SI). A statistically significant but weak negative size dependence was found across the full clinical size range of 1 to 10 µm and 1 to 5 µm (See Table S1 for Pearson's and Spearman's coefficients), indicating that as microbubble size decreased, GP tended to increase slightly. For microbubbles ranging from 6 to 10 µm no statistically significant relationship between size and GP was seen.

Histograms of microbubble size distributions are presented below the GP lines (Figure S2). DSPC and DSEPC microbubbles had similar size distributions with a peak diameter around 3 µm, whereas both DPPC and SonoVue exhibited broader size distributions with a greater proportion of microbubbles larger than 6 µm. It was also seen that larger microbubbles were more susceptible to phase separation, with distinct areas of low and high lipid order being observed (Figure S3). Such phase separation may also exist within the size range investigated here but regions may not be of sufficient area to be resolvable with the setup used in this study.

***Table 2**. Weighted mean GP values from n=3 repeats. Mean GP values are given with the pooled standard deviation. The total number of bubbles used per formulation, i.e. for all 3 repeats, to generate GP statistics are given. Mean GP values and standard deviations (via pooling) have been weighted by number of microbubbles per repeat, to give the final statistic.*

Formulation	Weighted mean GP	Pooled standard deviation	Total microbubbles processed
DPPC	0.468	0.050	1050
DSEPC	0.509	0.056	2284
DSPC	0.483	0.056	1767
SonoVue	0.494	0.053	949
D-L	0.523	0.061	3828

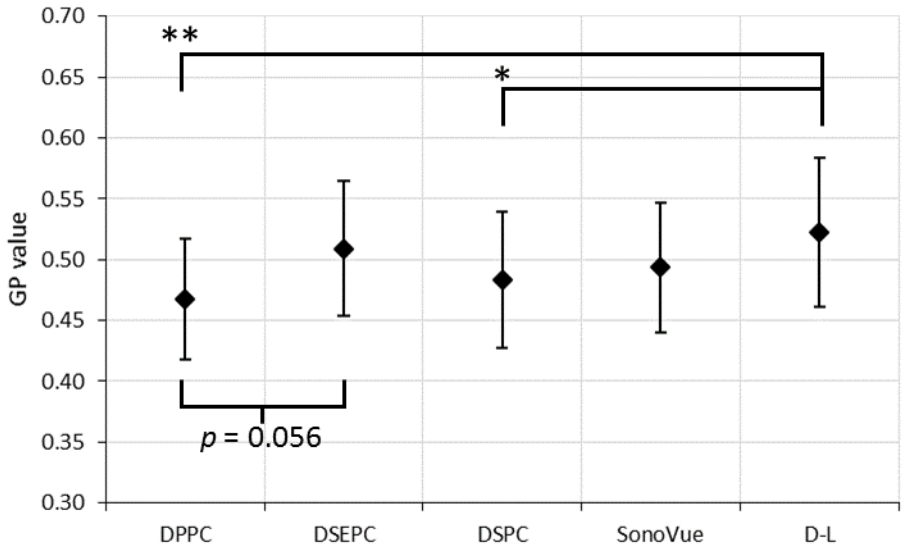

*Figure 3: Mean GP values for different formulations at the ambient temperature and pressure. The error given is a pooled standard deviation for the 3 repeats per formulation. Mean GP values are weighted by number of microbubbles (see Table 2). *p<0.05, **p<0.01. Confidence intervals are given in Figure S6.*

Lipid order of microbubbles compared to liposomal solutions

Despite the range of lipids employed in this study, the GP values for all of the microbubble formulations tested was very similar, indicating similar lipid order. As will be discussed later, it was hypothesized that this was due to the high Laplace pressure and the resulting lateral compression of the kinetically trapped lipids at the microbubble surface. To test this, the GP of both DPPC microbubbles and DPPC liposomes was assessed in the flow chamber setup. If the hypothesis is correct then the liposomes should have exhibited a lower GP. This experiment was performed under static conditions and without ultrasound exposure. The liposomes were indeed found to have a lower GP (0.159 ± 0.035) than either the unwashed microbubbles (0.240 ± 0.05) or the washed microbubbles (0.300 ± 0.012) (Figure 4). That the washed microbubbles had a significantly higher average GP than the unwashed microbubbles may be due to the presence of liposomes and other non-gas-filled lipid structures in the unwashed microbubble solution. For all subsequent experiments with the flow chamber setup, microbubbles were washed by the method described above prior to ultrasound exposure and/or GP measurement to prevent any contaminating lipid debris from influencing the dynamic GP measurements of the microbubbles.

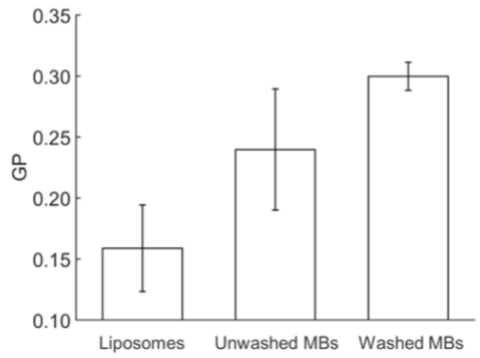

Figure 4: The GP of C-Laurdan-labelled solutions of lipids (liposomes), unwashed microbubbles, and washed microbubbles were compared using the flow chamber setup under static conditions at 37°C (n = 3). The GP values of the 3 conditions were found to be significantly different (p < 0.01) by a one-way ANOVA followed by Tukey-Kramer post-hoc comparisons.

Simultaneous measurement of microbubble acoustic emissions and lipid order under ultrasound exposure

Having determined that gas-filled DPPC microbubbles had a higher lipid order than liposomal DPPC vesicles, and that acoustic emissions monitoring could be employed to track the destruction of the DPPC microbubbles, the flow chamber setup was employed to evaluate the impact of ultrasound exposure on the lipid order of washed microbubbles using simultaneous acoustic emissions monitoring and dynamic GP measurements.

The results revealed a statistically significant ($p < 0.01$) decrease in the GP of C-Laurdan following the destruction of the microbubbles by ultrasound (from 0.300 ± 0.012 to 0.277 ± 0.016, $n = 11$, see Figure 5). Additionally, this decrease was temporally resolved for those samples that were adequately aligned, enabling comparison of the dynamic GP measurements taken during ultrasound exposure with the measured acoustic emissions. It was found that the decrease in GP of the microbubble solution exposed to ultrasound corresponded with the application of ultrasound and correlated with the decrease in acoustic emissions as the microbubbles were destroyed (see Figure 5b-c). Notably, no subsequent recovery of the microbubble GP to pre-exposure levels was detected in any of the samples during the measurement period spanning several minutes.

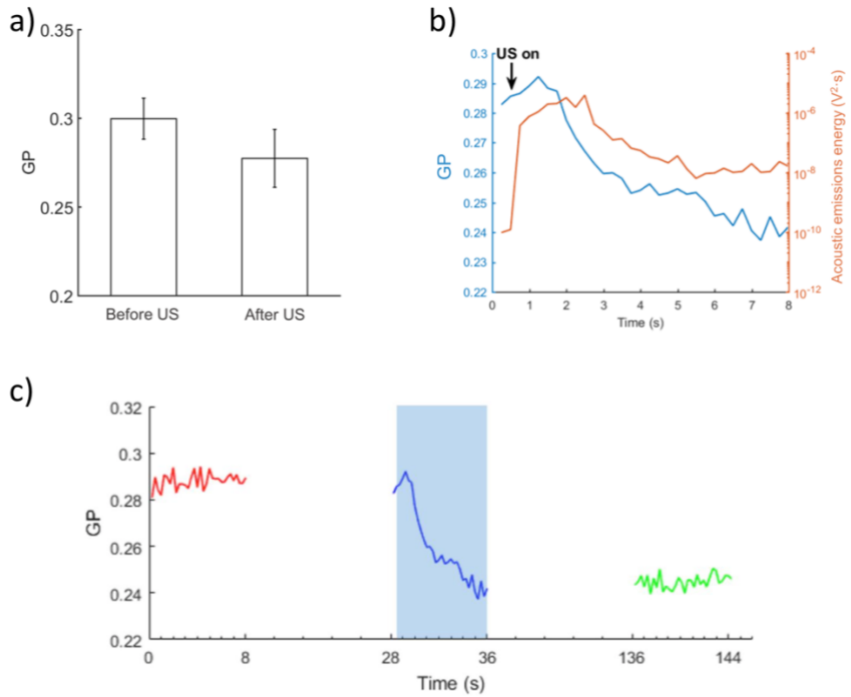

Figure 5: Simultaneous acoustic emissions monitoring and dynamic GP measurements throughout exposure of DPPC microbubbles to ultrasound in the flow chamber setup at at 37°C. A) GP of DPPC microbubbles before and after ultrasound exposure, a significant difference ($p < 0.01$) in the GP value was observed, as determined by an unpaired t-test. Bars indicate mean ± standard deviation. n = 11. B) Dynamic GP measurements (blue, left axis), and energy of acoustic emissions relative to control (orange, right axis) for DPPC microbubbles exposed to ultrasound. C) Temporally-resolved GP of DPPC microbubbles before ultrasound exposure (red), during ultrasound exposure (blue shaded region), and after ultrasound exposure (green).

Single bubble acoustic response

The oscillatory behaviour of single microbubbles of four of the formulations was investigated using the acoustic/optical setup described above. As shown in Figure 6A all microbubbles exhibited a similar median expansion over the course of the 5 cycle pulse, that increased with driving pressure. In addition, a change in microbubble size before and after ultrasound was observed that also increased with driving pressure (Figure 6B), likely due to microbubble destruction and increased gas dissolution. Despite the differences in the formulations, no significant differences were seen in the behaviour or stability of the microbubbles under ultrasound exposure.

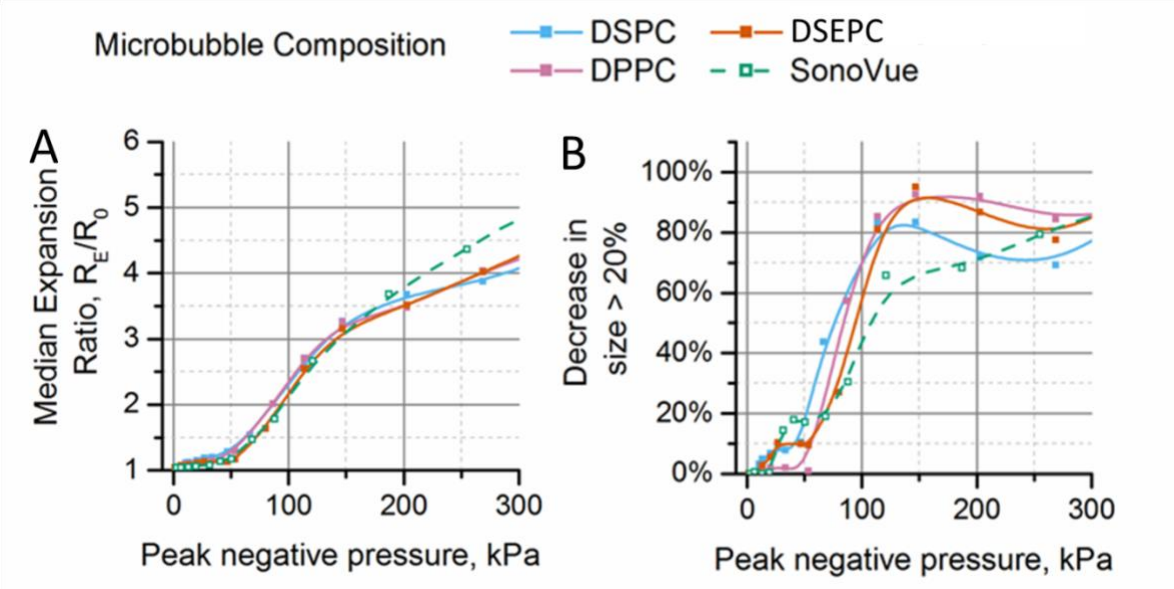

Figure 6: Acoustic behaviour of microbubbles of different lipid compositions as determined by Mie scattering of single microbubbles at the focus of a 3.5 MHz transducer in water at ambient temperature and pressure. Microbubbles underwent increasing (A) radial expansion as pressure increased. In addition, (B) the proportion of microbubbles, given on the y-axis, experiencing a decrease in size >20% over the ultrasound pulse, increased with increasing pressure. Each data point is the median of a minimum of 100 microbubbles.

DISCUSSION

Effects of microbubble formulation on lipid order

All of the experiments in this study were conducted at temperatures below the gel to liquid transition temperature of the primary lipids used in the formulations. Thus the influence of phosphatidylcholine hydrocarbon chain length upon lipid order was expected to be relatively modest [25-26]. Nevertheless, at any given pressure and temperature, lipids with shorter chains will have more energy per conformational degree of freedom compared to those with longer chains and, in non-gas-filled lipid structures such as liposomes and micelles, this has been shown to give rise to more disordered membranes [27-29]. It is thus interesting that the differences in GP between DSEPC, DPPC, DSPC and SonoVue microbubbles in Figure 3 were not statistically significant.

There was found to be a small statistically significant difference in GP between D-L and DPPC and DSPC microbubbles. Considering that D-L microbubbles consist primarily of DPPC (80% by molarity), this indicates that the phosphatidylcholine hydrocarbon chain length and head group charge are not the only factors influencing lipid order, and that the emulsifier and/or preparation method, can also affect microbubble shell properties. Unlike DPPC or DSPC microbubbles, D-L microbubbles contain DSPE-5K, as an emulsifying agent, and DPPA. DPPA lacks the bulky choline molecule headgroup found on DPPC or DSPC, and is typically negatively charged under physiological conditions. Differences in the size of the PEG moiety are known to affect lipid order, along with the relative concentrations of the PEG-lipid molecule to the main lipid [29]. The suspending medium may also influence lipid order by affecting the hydration of the membrane. The use of a water, propylene glycol and glycerol mixture, even after dilution in water during staining, may alter the membrane hydration by changing the osmotic balance between the membrane and the solution, or by interacting with water molecules or choline headgroups at the interface.

Dominance of surface tension in determining microbubble lipid order

Across all of the different MB formulations tested in this study, the mean GP only varied between 0.468 to 0.523, a range of 0.055. Between DSPC and DPPC microbubbles, the difference was just 0.015. In comparison, there was a difference of ~0.047 between the DSPC and DPPC liposome suspensions (Figure S4c). One explanation for this is that the Laplace pressure due to surface tension at the gas-liquid interface of the microbubble will be much higher than at the liquid-liquid interface of the liposome. Thus, the microbubble shell will experience much higher lateral compression and hence exhibit much higher lipid order; to the extent that the effects of composition, hydration etc. are secondary. This also explains the similarity in the acoustic response of the different formulations (Figure 6). For a given set of ultrasound conditions, microbubble dynamics will be determined primarily by microbubble diameter and the effective shear elasticity and viscosity of the shell, which in turn will be proportional to the lipid order [8]. Further supporting evidence is provided by the real-time measurements of GP made during ultrasound exposure of the microbubbles (Figure 5). These showed that GP fell simultaneously with the amplitude of the acoustic emissions, indicating that the lipid order of the debris produced by microbubble destruction was lower than that of the original microbubbles. This has potentially interesting implications for therapeutic applications of microbubbles. Recent studies have indicated that transfer of material from microbubbles to biological membranes may be important for therapeutic applications[30-31]. Thus, it might be possible to utilise lipids to generate vesicles upon microbubble destruction that could enhance membrane permeabilization for drug delivery.

Correlation between microbubble stability and lipid order

As lipid hydrocarbon chain length increases, both the stiffness of the lipid shell and the diffusion distance are expected to increase, resulting in a decrease in the permeability of the lipid shell, and improved microbubble stability [32]. Both Borden et al. [33] and Carugo et al. [30] found that microbubble stability increased with increasing lipid chain length. It is perhaps surprising therefore that no statistically significant difference in stability was observed between DPPC and DPSC bubbles in Figure 2. The fact that D-L microbubbles, which also consist primarily of DPPC, did not exhibit the same stability as DPPC microbubbles indicates, however, that lipid chain length is not the only determinant of shell permeability. The results suggest instead that all of the factors affecting lipid order discussed above - choice of emulsifier, buffer, and the relative concentrations of the formulation constituents - need to be taken into account.

Other considerations

Stability and acoustic response are not the only factors influencing the selection of microbubble composition. For clinical applications, the immunogenicity of the microbubbles and the potential for attaching targeting or therapeutic species are also important. Spectral imaging may provide a useful technique for determining the availability and/or uniformity of binding sites on microbubble surfaces. It is also useful in determining the uniformity of the microbubbles themselves within a population or for example between batches for different experiments. The fact that there was seen to be considerable variability in the lipid order of individual microbubbles within each formulation (Table 2 and Figure 3) suggests that the manufacturing technique used in this study could be improved.

Limitations and further work

An important limitation of the present study concerns the minimum microbubble size that can be detected with the various experimental techniques employed. For counting and sizing microbubbles by electrozone sensing, the smallest object that can be detected is 0.4 μm. For the experiments employing spectral imaging by confocal microscopy, circular objects with considerable fluorescence in their centres, possibly from contamination, microbubble deflation, or out-of-plane fluorescence, were excluded from the analysis because they could not be confirmed as microbubbles. Microbubbles below ~2.5 μm in diameter were particularly challenging to confirm as the image resolution results in microbubbles with a diameter of <10 pixels (1 pixel = 0.264 μm). In addition, the confocal pinhole size used has a z-axis focal plane of 0.8 μm, which can introduce curvature effects from microbubble shells. As such, it can be difficult to confirm a gaseous space within small microbubbles due to overlapping fluorescence. In the single bubble acoustic measurements, microbubbles with diameters smaller than 2 μm were also excluded on the basis of the limiting criteria for detection set out in Rademeyer et al. [14].

With regard to the high-speed GP measurements, the PMTs captured fluorescence emissions for the entire field of view. The GP recorded was therefore an average across all the C-Laurdan-labelled material in the field of view and may have included lipids in different order environments, despite an ability to identify those structures (e.g. small microbubbles) by camera. This may explain the difference in lipid order between the pure lipid solution and the destroyed microbubbles after ultrasound exposure. Similarly, since the microbubbles in that experiment were only destroyed at the ultrasound focus, it is possible that microbubbles too small to identify by camera diffused into the area captured by the PMTs.

CONCLUSION

Spectral imaging was found to be an effective method for characterising microbubble surface properties under both static and dynamic conditions. Microbubble stability, lipid order and acoustic response were examined for five microbubble formulations intended to represent those most commonly employed in both research and clinical agents.

A surprising consistency in lipid order, irrespective of microbubble size or composition, was found across the formulations tested. In addition, it was found that microbubbles exhibited a higher lipid order than that of liposomes of the same lipid composition; and similarly, that the mean lipid order of microbubble suspensions was seen to decrease upon exposure to ultrasound resulting in microbubble destruction. These results together suggest that microbubble lipid order is influenced more strongly by surface tension than composition. This finding also explains the similarity in the acoustic response of individual microbubbles of different compositions, as the dynamic behaviour of microbubbles of a given size is expected to be determined by the viscoelastic properties of the shell and hence the surface molecular concentration.

Lipid order was not found to be a good predictor of microbubble stability, likely because the combination of hydrocarbon chain length, lipid head group size and charge, and the selection of emulsifier and suspending medium were also important. Future work using this technique could investigate the relative impact of individual components.

Although the variation in lipid order between different formulations was found to be small, there was considerable variability in both lipid order and acoustic response between individual microbubbles within each formulation. This suggested that improvements to the manufacturing technique could be made to improve microbubble uniformity and that this could be assessed via spectral imaging.

ACKNOWLEDGEMENTS

The authors would like to acknowledge James Fisk and David Salisbury for their contribution to the design and construction of the experimental apparatus used in this work. Funding for the work was provided by the Engineering and Physical Sciences Research Council (EP/I021795/1 and EP/L024012/1) and the Institute of Engineering and Technology (AF Harvey Prize).

REFERENCES

1. Sirsi, S.; Borden, M., Microbubble compositions, properties and biomedical applications. *Bubble Science, Engineering & Technology* **2009,** *1* (1-2), 3-17.
2. Masugata, H.; Peters, B.; Lafitte, S.; Strachan, G. M.; Ohmori, K.; DeMaria, A. N., Quantitative assessment of myocardial perfusion during graded coronary stenosis by real-time myocardial contrast echo refilling curves. *Journal of the American College of Cardiology* **2001,** *37* (1), 262-269.
3. Wei, K.; Jayaweera, A. R.; Firoozan, S.; Linka, A.; Skyba, D. M.; Kaul, S., Quantification of Myocardial Blood Flow With Ultrasound-Induced Destruction of Microbubbles Administered as a Constant Venous Infusion. *Circulation* **1998,** *97* (5), 473-483.
4. Song, H.-P.; Yu, M.; Zhang, M.; Han, Z.-H.; Zhang, H.-B.; Zhu, T.; Zhou, X.-D., Diagnosis of Active Hemorrhage From the Liver With Contrast-Enhanced Ultrasonography After Percutaneous Transhepatic Angioplasty and Stent Placement for Budd-Chiari Syndrome. *Journal of Ultrasound in Medicine* **2009,** *28* (7), 955-958.
5. Wei, K.; Jayaweera, A. R.; Firoozan, S.; Linka, A.; Skyba, D. M.; Kaul, S., Basis for detection of stenosis using venous administration of microbubbles during myocardial contrast echocardiography: Bolus or continuous infusion? *Journal of the American College of Cardiology* **1998,** *32* (1), 252-260.
6. Unger, E.; Porter, T.; Lindner, J.; Grayburn, P., Cardiovascular drug delivery with ultrasound and microbubbles. *Advanced Drug Delivery Reviews* **2014,** *72*, 110-126.
7. Rychak, J. J.; Klibanov, A. L., Nucleic acid delivery with microbubbles and ultrasound. *Advanced drug delivery reviews* **2014,** *72*, 82-93.
8. Marmottant, P.; van der Meer, S.; Emmer, M.; Versluis, M.; de Jong, N.; Hilgenfeldt, S.; Lohse, D., A model for large amplitude oscillations of coated bubbles accounting for buckling and rupture. *The Journal of the Acoustical Society of America* **2005,** *118* (6), 3499-3505.
9. Chomas, J. E.; Dayton, P.; Allen, J.; Morgan, K.; Ferrara, K. W., Mechanisms of contrast agent destruction. *IEEE Transactions on Ultrasonics, Ferroelectrics and Frequency Control* **2001,** *48* (1), 232-248.
10. Duncan, P. B.; Needham, D., Test of the Epstein−Plesset Model for Gas Microparticle Dissolution in Aqueous Media: Effect of Surface Tension and Gas Undersaturation in Solution. *Langmuir* **2004,** *20* (7), 2567-2578.
11. Hosny, N. A.; Mohamedi, G.; Rademeyer, P.; Owen, J.; Wu, Y.; Tang, M.-X.; Eckersley, R. J.; Stride, E.; Kuimova, M. K., Mapping microbubble viscosity using fluorescence lifetime imaging of molecular rotors. *Proceedings of the National Academy of Sciences* **2013,** *110* (23), 9225-9230.
12. Kooiman, K.; Emmer, M.; Kokhuis, T. J. A.; Bosch, J. G.; de Gruiter, H. M.; van Royen, M. E.; Van Cappellen, W. A.; Houtsmuller, A. B.; Van der Steen, A. F. W.; de Jong, N. In *Lipid distribution and*

viscosity of coated microbubbles, Ultrasonics Symposium (IUS), 2010 IEEE, 11-14 Oct. 2010; 2010; pp 900-903.
13. Borden, M. A.; Martinez, G. V.; Ricker, J.; Tsvetkova, N.; Longo, M.; Gillies, R. J.; Dayton, P. A.; Ferrara, K. W., Lateral Phase Separation in Lipid-Coated Microbubbles. *Langmuir* **2006,** *22* (9), 4291-4297.
14. Rademeyer, P.; Carugo, D.; Lee, J. Y.; Stride, E., Microfluidic system for high throughput characterisation of echogenic particles. *Lab on a Chip* **2015,** *15* (2), 417-428.
15. Sezgin, E.; Levental, I.; Grzybek, M.; Schwarzmann, G.; Mueller, V.; Honigmann, A.; Belov, V. N.; Eggeling, C.; Coskun, Ü.; Simons, K.; Schwille, P., Partitioning, diffusion, and ligand binding of raft lipid analogs in model and cellular plasma membranes. *Biochimica et Biophysica Acta (BBA) - Biomembranes* **2012,** *1818* (7), 1777-1784.
16. Sezgin, E.; Sadowski, T.; Simons, K., Measuring Lipid Packing of Model and Cellular Membranes with Environment Sensitive Probes. *Langmuir* **2014,** *30* (27), 8160-8166.
17. Kwiatek, J. M.; Owen, D. M.; Abu-Siniyeh, A.; Yan, P.; Loew, L. M.; Gaus, K., Characterization of a New Series of Fluorescent Probes for Imaging Membrane Order. *PLOS ONE* **2013,** *8* (2), e52960.
18. Parasassi, T.; De Stasio, G.; d'Ubaldo, A.; Gratton, E., Phase fluctuation in phospholipid membranes revealed by Laurdan fluorescence. *Biophys J* **1990,** *57* (6), 1179-86.
19. Dodes Traian, M. M.; Gonzalez Flecha, F. L.; Levi, V., Imaging lipid lateral organization in membranes with C-laurdan in a confocal microscope. *J Lipid Res* **2012,** *53* (3), 609-16.
20. Shrivastava, S.; Cleveland, R. O.; Schneider, M. F., On measuring the acoustic state changes in lipid membranes using fluorescent probes. *Soft Matter* **2018,** *14* (47), 9702-9712.
21. Sanchez, S. A.; Tricerri, M. A.; Gratton, E., Laurdan generalized polarization fluctuations measures membrane packing micro-heterogeneity in vivo. *Proceedings of the National Academy of Sciences of the United States of America* **2012,** *109* (19), 7314-7319.
22. Feshitan, J. A.; Chen, C. C.; Kwan, J. J.; Borden, M. A., Microbubble size isolation by differential centrifugation. *J Colloid Interface Sci* **2009,** *329* (2), 316-24.
23. Sezgin, E.; Waithe, D.; Bernardino de la Serna, J.; Eggeling, C., Spectral Imaging to Measure Heterogeneity in Membrane Lipid Packing. *Chemphyschem* **2015,** *16* (7), 1387-1394.
24. Schneider, M., SonoVue, a new ultrasound contrast agent. *European Radiology* **1999,** *9*, S347-S348.
25. Bagatoll, L. A.; Parasassi, T.; Fidelio, G. D.; Gratton, E., A Model for the Interaction of 6-Lauroyl-2-(N,N-dimethylamino)naphthalene with Lipid Environments: Implications for Spectral Properties. *Photochemistry and Photobiology* **1999,** *70* (4), 557-564.
26. Zorila, B.; Bacalum, M.; Popescu, A.; Radu, M., *Log-normal deconvolution of laurdan fluorescence spectra – A tool to assess lipid membrane fluidity*. 2016; Vol. vol 68, p 702-712.
27. Bagatolli, L. A.; Gratton, E., Direct Observation of Lipid Domains in Free-Standing Bilayers Using Two-Photon Excitation Fluorescence Microscopy. *Journal of Fluorescence* **2001,** *11* (3), 141-160.
28. Marsh, D., Structural and thermodynamic determinants of chain-melting transition temperatures for phospholipid and glycolipids membranes. *Biochimica et Biophysica Acta (BBA) - Biomembranes* **2010,** *1798* (1), 40-51.
29. Kenworthy, A. K.; Simon, S. A.; McIntosh, T. J., Structure and phase behavior of lipid suspensions containing phospholipids with covalently attached poly(ethylene glycol). *Biophysical Journal* **1995,** *68* (5), 1903-1920.
30. Carugo, D.; Aron, M.; Sezgin, E.; Bernardino de la Serna, J.; Kuimova, M. K.; Eggeling, C.; Stride, E., Modulation of the molecular arrangement in artificial and biological membranes by phospholipid-shelled microbubbles. *Biomaterials* **2017,** *113*, 105-117.
31. De Cock, I.; Lajoinie, G.; Versluis, M.; De Smedt, S. C.; Lentacker, I., Sonoprinting and the importance of microbubble loading for the ultrasound mediated cellular delivery of nanoparticles. *Biomaterials* **2016,** *83*, 294-307.

32. Nagle, J. F.; Scott, H. L., Lateral compressibility of lipid mono- and bilayers. Theory of membrane permeability. *Biochimica et Biophysica Acta (BBA) - Biomembranes* **1978,** *513* (2), 236-243.
33. Borden, M. A.; Longo, M. L., Dissolution Behavior of Lipid Monolayer-Coated, Air-Filled Microbubbles: Effect of Lipid Hydrophobic Chain Length. *Langmuir* **2002,** *18* (24), 9225-9233.

TABLE OF CONTENTS GRAPHIC